ACTUATORS

Cavatappi artificial muscles from drawing, twisting, and coiling polymer tubes

Diego R. Higueras-Ruiz, Michael W. Shafer*, Heidi P. Feigenbaum

Compliant, biomimetic actuation technologies that are both efficient and powerful are necessary for robotic systems that may one day interact, augment, and potentially integrate with humans. To this end, we introduce a fluid-driven muscle-like actuator fabricated from inexpensive polymer tubes. The actuation results from a specific processing of the tubes. First, the tubes are drawn, which enhances the anisotropy in their microstructure. Then, the tubes are twisted, and these twisted tubes can be used as a torsional actuator. Last, the twisted tubes are helically coiled into linear actuators. We call these linear actuators cavatappi artificial muscles based on their resemblance to the Italian pasta. After drawing and twisting, hydraulic or pneumatic pressure applied inside the tube results in localized untwisting of the helical microstructure. This untwisting manifests as a contraction of the helical pitch for the coiled configuration. Given the hydraulic or pneumatic activation source, these devices have the potential to substantially outperform similar thermally activated actuation technologies regarding actuation bandwidth, efficiency, modeling and controllability, and practical implementation. In this work, we show that cavatappi contracts more than 50% of its initial length and exhibits mechanical contractile efficiencies near 45%. We also demonstrate that cavatappi artificial muscles can exhibit a maximum specific work and power of 0.38 kilojoules per kilogram and 1.42 kilowatts per kilogram, respectively. Continued development of this technology will likely lead to even higher performance in the future.

INTRODUCTION

Traditional electric and fluidic actuators operate effectively in many tasks, yet their complexity and rigid configuration often limit their deployment in areas such as biomimetic robotics and compliant structures and limit the design space of their host system. This has driven research into alternative solid-state, flexible actuators, but the challenge has been producing high specific power metrics while maintaining the efficiency, form factor, and predictable performance necessary for adoption. The key metrics often used for soft actuator selection in applications are average and peak specific power, specific work, maximum actuation strain and stress, lifetime, and actuator efficiency. Many of these metrics are governed by the input driver of the actuator, for example, electrically or fluidically driven actuators tend to be much more efficient than thermally driven actuators.

To help compare different soft actuator technologies, Table 1 summarizes key metrics of several soft-actuators and human muscle, which many of these actuators aim to mimic, and provides total system efficiency metrics that consider the electric energy to mechanical work conversion (chemical free energy to mechanical work for human muscles). Included in this table are thermally activated twisted polymer actuators (TPAs), which are made from inexpensive fibers, such as fishing line. TPAs have been shown to develop a specific work of 2.48 kJ/kg and an average specific power of 27.1 kW/kg (*1*); however, their thermal activation limits response time, controllability, and efficiency. The electric-mechanical energy conversion efficiency for TPAs is thought to be similar to that presented for shape-memory alloys, which is about 1 to 2% (*1*).

McKibben actuators are pneumatically or hydraulically driven artificial muscles (PAMs or HAMs) widely used in robotics (*2*, *3*). They change length by inflating a bladder that is surrounded by a counter double-helix–braided sheath. The macroscopically developed anisotropy allows the device to contract in length and expand radially (*4*). Pleated pneumatic artificial muscles (PPAMs) are a recently improved incarnation of the conventional McKibben actuator that can develop a specific work of 1.1 kJ/kg, an average specific power of 1 kW/kg, and contractions of 38% (*5*, *6*). Small McKibbens can be fabricated with dimensions on the order of a few millimeters in diameter (*7*), yet at both large and small scales, their multicomponent nature causes frictional losses and hysteresis, which has frustrated the development of accurate models that would allow precise control algorithms (*8*), although this has been reduced in PPAMS. But for all McKibbens, during actuation, their diameter increases as a result of the inflation that drives their actuation. These radial changes make parallel operation volumetrically inefficient.

To improve some of the McKibbens drawbacks, new actuator designs have been presented such as pouch motors, fluid-driven origami-inspired artificial muscles (FOAMs), and origami-based vacuum pneumatic artificial muscles (OV-PAMs). Pouch motors are fabricated from bonded films that form an inflatable planar pouch that can be connected in series, forming paired pouch motors. This configuration can develop contractions of 31% with payloads of 10 kg when the pouches are pressurized (*9*, *10*). Although paired pouch motors are mentioned here and can be used in soft robotics, these do not appear in Table 1 because nondimensional or specific metrics have not been directly reported in the literature. Both FOAMs and OV-PAMs are origami-based vacuum-actuated actuators. The former uses a skeleton with a repeated zigzag pattern in a sealed bag. When negative pressure is applied to the actuator, the air within exits the bag, and the zigzag pattern leads to the contractile deformation of the actuator. These actuators develop contractions of up to ~90% and a mechanical-to-mechanical energy conversion contractile efficiency of 23 and 59% when pneumatically and hydraulically tested, respectively. However, the great generated contractions by FOAMs substantially decrease with small actuation load increments (*11*). The related OV-PAMs consist of a sealed film chamber made from polyvinyl chloride (PVC) connecting a top and a bottom plate

Department of Mechanical Engineering, Northern Arizona University, 2112 S. Huffer Lane., Flagstaff, AZ 86011, USA.
*Corresponding author. Email: michael.shafer@nau.edu

Table 1. Comparison of metric for various soft actuators. Dash entries indicate data not found.

Metric	Cavatappi (*37–40*)	TPA (*1*)	PPAM (*5, 6, 41*)	HASEL (*14, 15*)	OV-PAM (*12, 13*)	FOAM (*11*)	Human muscle (*42, 43*)
Avg/peak specific power* (kW/kg)	0.8 / 1.42	27 / 50	1 / –	0.36 / 0.59	– / 0.02	~1 / ~2	0.05 / 0.28
Specific work (kJ/kg)	0.11–0.38	2.48	1.1	0.07	0.19	~0.25	0.04
Maximum actuation Strain (%)	~50	49	38	~60	>90	90	>40
Maximum actuation stress (MPa)	~0.70	~100	0.67	0.3	0.04	~0.6	0.35
Lifetime (cycles)	$>10^{4}$†	$>10^{6}$	$>10^{5}$	$>10^{5}$	–	$>10^{4}$	$>10^{9}$
Actuator efficiency (%)	~9‡§ and ~45‡‖	–	~57‡‖	–	~99‡§	23‡§ and 59‡‖	–
Total system efficiency (%)	10–22‡‖	~1	~5‡‖	21‖¶	16‡§	2–5‡§	~20

*This value is limited to the energy rate provided by the energy source. †This was the maximum number of cycles tested, not an upper limit on lifetime. Cavatappi showed no signs of degradation. ‡Actuators' energy conversion contractile efficiency (without energy recovery). §Pneumatic. ‖Hydraulic. ¶Full-cycle analysis of actuator efficiency (includes energy recovery).

with evenly spaced transverse reinforcements. The previously mentioned actuation strain-stress ratio limitation of FOAMs is solved with OV-PAMS because they can keep an actuation strain close to 100% while generating their maximum actuation force. However, OV-PAMs are voluminous, which could limit their implementation in small robotic applications (*12*, *13*).

The previously mentioned actuators are all thermally or fluidically driven; hydraulically amplified self-healing electrostatic actuators (HASELs) are electrohydraulic activated. These muscle-mimetic actuators are fabricated from an elastomeric shell partially covered by a pair of opposing electrodes and filled with a dielectric liquid. Upon voltage application, the induced electric field generates an electrostatic Maxwell stress that pressurizes and displaces the liquid dielectric leading to the actuator's contraction. HASELs can generate actuation strains of about 60% (calculated as the actuator contraction displacement divided by the actuator initial length) and full-cycle electric-mechanical efficiency of 21% (see Table 1). However, these actuators require high voltage (>5 kV) and have thus required voluminous power electronics in testing (*14*, *15*).

Here, we present an actuation mechanism that is a hybrid of TPAs and McKibben actuators, which we have named cavatappi, after the Italian pasta with similar shape (see Fig. 1A). Cavatappi exploits the material's anisotropic microstructure to develop actuation like TPAs, yet they are pneumatically/hydraulically driven like McKibben actuators. The anisotropic microstructure is developed through drawing of inexpensive polymer tubes. After drawing, the tubes are twisted and coiled like TPAs. Therefore, cavatappi have the simplicity and size of TPAs with the actuation response and mechanical efficiencies of McKibben actuators. Table 1 shows actuation characterization of single-component cavatappi artificial muscles as compared with the other soft actuators. Although sacrificing some performance of TPAs, cavatappi drastically increase others and in doing so, better meet or exceed the performance of skeletal human muscle in many key metrics. With specific peak power metrics of ~1.4 kW/kg, cavatappi exceeds the capacity of human muscle while maintaining a mechanical conversion efficiency of ~45%. With actuation strains of up to 50% and minimal diametral changes during actuation, these devices can be placed in parallel to increase actuation force akin to biological muscle fibers. Because of their cost, performance, ease of fabrication, and compliant form, cavatappi fit the needs of many current and future robotic actuation applications.

Design and development of cavatappi

The design and development of cavatappi was originally inspired by the mechanics of TPAs, particularly the idea of exploiting the material's anisotropy to generate actuation (*1*). TPAs are thermally driven linear or torsional actuators, whose actuation response is a result of the anisotropic thermal properties of the precursor (untwisted) material, which experiences axial thermal contraction and radial thermal expansion. They are inexpensive, often fabricated from fishing line, and have been demonstrated in areas such as robotics (*16–18*), medical devices (*19*), and active textiles (*1*, *20*). In the past few years, our team has focused its effort on understanding the actuation mechanism of TPAs and how TPAs' actuation can be modeled using the material properties of the precursor fibers (*21–23*). As part of this work, we found the standard TPA materials to be highly viscoelastic (*24–26*) and hygroscopic, which causes their response/performance to depend on moisture content (*27*). Moreover, the viscoelastic and hygroscopic properties of TPAs are strongly affected by temperature changes, and temperature changes are required for actuation. This makes TPAs challenging to model and therefore control (*21–23*, *28–30*). Last, thermal activation is generally an inefficient and time-consuming (particularly during cooling) driver.

The extreme performance and shortcomings of TPAs led our team to explore alternative actuation modalities that might mitigate inherent drawbacks yet take advantage of their strengths by mimicking their actuation mechanism. We surmised that internal pressure in a tube could be used to develop similar anisotropic expansion seen during TPA heating and initially tested straight extruded/drawn tubes of polymers. Pressure testing showed that soft PVC tubing (Fig.1B, left) was able to generate radial expansion similar to TPAs,

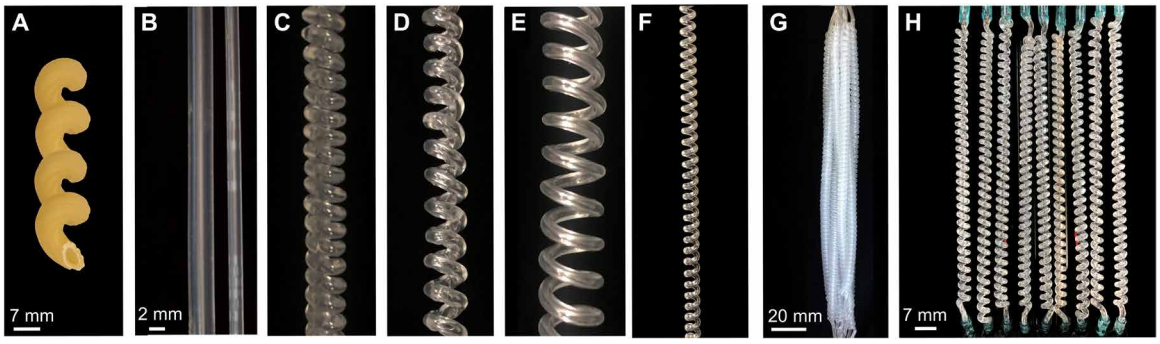

Fig. 1. Cavatappi pasta, cavatappi artificial muscles, and precursor tubes. (**A**) Cavatappi pasta is shaped as a helical tube yet lacks the anisotropic material properties necessary to be deployed as an effective actuator. (**B**) Precursor undrawn tube (left, 3.18 mm *OD* and 1.58 mm *ID*) and precursor drawn tube (right, 1.8 mm *OD* and 0.85 mm *ID*). (**C**) Cavatappi made from a 1.8-mm-*OD*/0.85-mm-*ID* tube. (**D**) Cavatappi in (B) that has been prestretched and annealed after fabrication to increase the helix pitch. (**E**) Cavatappi made from the drawn precursor tube shown in (B) and coil *ID* of 7 mm. (**F**) Mini-cavatappi made from a 0.7-mm-*OD*/0.25-mm-*ID* tube. (**G**) Bundle of cavatappi artificial muscles that simulate a human skeletal muscle bundle. (**H**) Linear-parallel configuration of nine cavatappi from (C). The scale bar in (B) is used for (B) to (F), and the scale bars for (A), (G), and (H) are shown in the figures. All tube diameters listed here are the drawn diameters.

yet the tubing developed axial expansion, which we knew from our TPA modeling would reduce actuation performance when twisted. Given the PVC microstructure, we set out to mitigate this axial expansion by enhancing anisotropy by cold drawing (Fig.1B, right) (*31*–*33*). Figure 1B shows the precursor tube [left, 3.18 mm outer dimater (*OD*) and 1.58 mm inside diameter (*ID*)] and the same tube (right, 1.8 mm *OD* and 0.85 mm *ID*) after the cold drawing necessary to increase axial stiffness relative to radial stiffness. Note the substantial change in diameter that occurs during the drawing process. We found that internal pressurization after drawing induced positive radial strains and negative axial strains that mimicked those of heated TPA precursor fibers. Next, we twisted these drawn tubes, which we knew from our work with TPA would reorient the high-stiffness molecular chains into a helical configuration around the central tube axis while maintaining the tube's ability to radially expand. Such a straight-twisted tube configuration would generate an untwisting when pressurized (torsional actuation). The twisted tubes were then helically coiled (Fig.1, C to H) so that the localized untwisting would manifest as linear actuation by reducing the coil's pitch. In this sense, the torsional actuators can be considered elemental units of the cavatappi (movie S1). Testing showed that the coiled configuration was able to lift weights, demonstrating the actuation phenomenon (see movie S2).

Once actuation was proven, other configurations of cavatappi were explored, see Fig. 1 (C to H), which includes prestretched cavatappi (Fig. 1, D to E), cavatappi with various coil diameters (Fig. 1E), mini-cavatappi made from smaller PVC tubing (Fig. 1F), and grouped cavatappi as bundled (Fig. 1G) or in parallel (Fig. 1, G and H). Here, we use the reinforced cavatappi artificial muscles with the configuration and dimensions shown in Fig. 1C and detailed in the Supplementary Materials (specifically, fig. S2) to characterize the actuation responses and performance properties of cavatappi artificial muscles, including actuation under various loads as a function of pressure and time, specific work, specific power, lifetime, creep, and actuator contractile efficiency. We also present some applications of cavatappi that demonstrate the use of prestretched cavatappi (similar to that in Fig. 1D) to increase the maximum actuation stroke, pairs or bundles (similar to that in Fig. 1, G and H) of cavatappi to increase the actuation contraction force, and mini-cavatappi (similar to that in Fig. 1F) for smaller-scale robots.

RESULTS

Mechanism of actuation

Cavatappi artificial muscles are fabricated from extruded polymer "precursor tubes" (Fig. 3, Fab. stage 1). During the extrusion process, the original material deforms into tubular structures, and anisotropy between the axial and hoop directions is induced. This extrusion process creates axially orientated tie molecules responsible for high axial strength (*33*). However, this anisotropy can be increased when the precursor tube is cold drawn, (Fig. 3, Fab. stage 2), by increasing the number of formed tie molecules (*31*, *32*).

To demonstrate the change in the anisotropic properties produced by drawing precursor tubes, we pressurized undrawn and drawn samples while measuring axial and radial strains (Fig. 2A). For the undrawn precursor tube, both axial and radial expansions show growth as a function of pressure, with axial changes of about 40% of the radial. After drawing this tube, the magnitude of radial expansion remains relatively unchanged but develops a more linear relationship with pressure. The axial response to pressure after drawing transitions from expansion to contraction, leading to a higher degree of anisotropy. The anisotropy of the material can be measured as the ratio of radial to axial strain or the difference between the radial and axial strain in response to pressure. The ratio highlights the sign changes of the expansions, and the difference is key in modeling of TPAs (*21*, *22*). At 175 psi, the undrawn tubes have an anisotropy ratio of about 2.4 and an anisotropy difference of about 12%. After drawing, the anisotropy ratio becomes about −31, and the difference becomes about 32%, highlighting the importance of drawing the tubes before fabrication of cavatappi artificial muscles. The positive radial strain and negative axial strains observed in the drawn tubes mirror the thermal response of TPA precursor fibers shown in Fig. 2B, which were reported by Swartz *et al.* (*21*). In this figure, we observe a similar negative anisotropy ratio and a large anisotropy difference, which is known to be the source of actuation in TPAs (*1*).

After drawing, the tubes can then be twisted to reorient the high-stiffness molecular chains into a helical configuration (Fig. 3, Fab. stage 3) so that internal pressurization generates an untwisting of the tube (Fig. 3, Act. stage 3, and movie S1). We think of sections of the twisted tubes as "elemental units" of the cavatappi because the localized shear deformation (untwist) is the fundamental actuation mechanism of the cavatappi muscle. The orientation of the

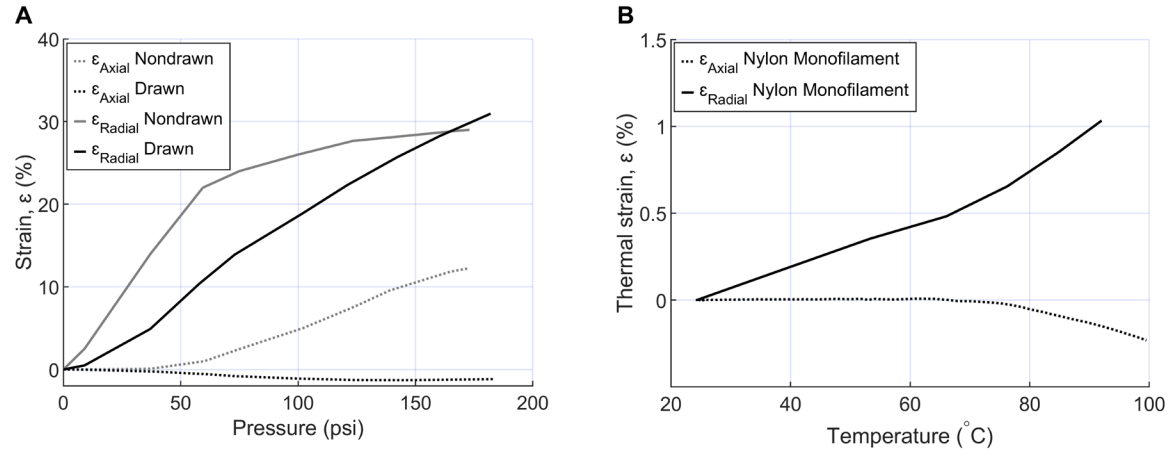

Fig. 2. Comparison of the axial and radial deformation for drawn and undrawn precursor tubes, as well as a nylon monofilament used for TPAs. (**A**) Axial and radial expansion of a drawn and undrawn precursor tubes as a function of pressure. Radial expansion response changes slightly after drawing, but axial direction switches from expansion to contraction. This response is similar to the axial and radial thermal expansion of a precursor nylon monofilament (**B**) used to make TPA. Note that drawn tubes in (A) show similar response to pressure as nylon monofilaments do to temperature in (B) where in the radial direction it expands, whereas in the axial direction it contracts. [Credit: Originally presented by Swartz *et al.* (*21*), IOP Publishing. Reproduced with permission. All rights reserved.]

twisted outer fiber is shown by the pitch angle, α, which is the angle between the original draw direction and the plane perpendicular to the longitudinal axis of the tube. If the tube is thin enough, then this pitch angle would be roughly constant through the tube wall thickness, but for thicker tubes, the pitch angle will vary radially, similar to TPAs. If the elemental unit is thermally annealed to release internal stresses, then the twisted configuration can be set. The actuation response of the elemental unit was tested under free torsion conditions, and the results are presented in section S4.

After twisting, a drawn tube can also be coiled (Fig. 3, Fab. stage 4) to create the final cavatappi artificial muscle. When this helical configuration is thermally annealed, the internal stresses are released, and this new shape holds after the loads that are used to maintain the configuration during the coiling process are removed. As a final step, as shown in Fig. 1D, the cavatappi may be prestretched to increase pitch before annealing. In these coiled configurations, when internal pressure is applied, the untwist in the elemental presents as helical contraction in the overall artificial muscle coil pitch (Fig. 3, Act. stage 4). We should note that the reinforcing monofilament of nylon 66 (used for increasing actuator stiffness and lifetime) is kept inside the tubular structure through the entire fabrication process and is thus also twisted and coiled. However, the monofilament used for reinforcement does no work during actuation, and any external loads on the cavatappi are not attached to the reinforcing filament. Thus, the reinforcement is solely there to increase the structural stability of the cavatappi.

Cavatappi artificial muscle: Actuation characterization

With the actuation phenomenon established, the motion of elemental segments discussed in section S4, and the dimensions and materials of the tested actuators presented in Materials and Methods, we present the cavatappi actuation response. Our testing to date has included actuations under various loads as a function of pressure and time; the latter illuminates viscoelastic effects. We have also developed tests to characterize specific work, specific power, lifetime, creep, and actuator contractile efficiency.

Force-strain-pressure and time response characterization

To develop an understanding of the actuation response under load, we conducted a series of isotonic actuation tests where pressure was cyclically ramped and tests where a step change of pressure was applied. The ramp test provided insights into how contraction depended on pressure, whereas the step change test informs bandwidth, specific power, and hints at how future dynamic models might be applied to these devices.

The isotonic actuation response of cavatappi to a ramped pressure input is shown in Fig. 4A. Here, we present the mean actuation results as a function of pressure, along with the 95% confidence intervals from data taken from trials on three different samples. For every test, four actuation cycles were executed. Each cycle included a 1.5-s ramp to 240 psi and a 2.5-s ramp back to atmospheric pressure. The data from the last cycle were used to calculate the average results plotted in Fig. 4A, as initial cycles exhibit some nonrecoverable deformation as the actuator is "worked in" (similar to the Mullins effect seen in many polymers).

The actuation strain shown in Fig. 4A generally increases as a power of pressure. This behavior is shown for all loads, except for the 0.1-kg mass where the nonlinear behavior stops after ~75 psi and appears more linear. In addition, this linear behavior stops for this mass at about 200 psi, where after the second derivative of strain in pressure becomes negative. We believe that this is because the coiled shape is completely saturated (there is little to no space between the coils of the helix) under these conditions.

Figure 4B shows the actuation of a cavatappi in response to a pressure step when loaded with a 400-g weight. Here, when plotted in the time domain, we can see an actuation contraction generated during the first ~0.25 s followed by an underdamped vibration. This ringing is expected from the elastic material properties, coiled shape of the muscle, and the dynamic loading of the actuator whose stiffness and equilibrium position are affected by the internal pressure.

Initially though, the actuation response of Fig. 4B consists of a dwell time of ~20 ms where pressure is increasing and actuation is not initiated. This is followed by the pressure-to-actuation time lag,

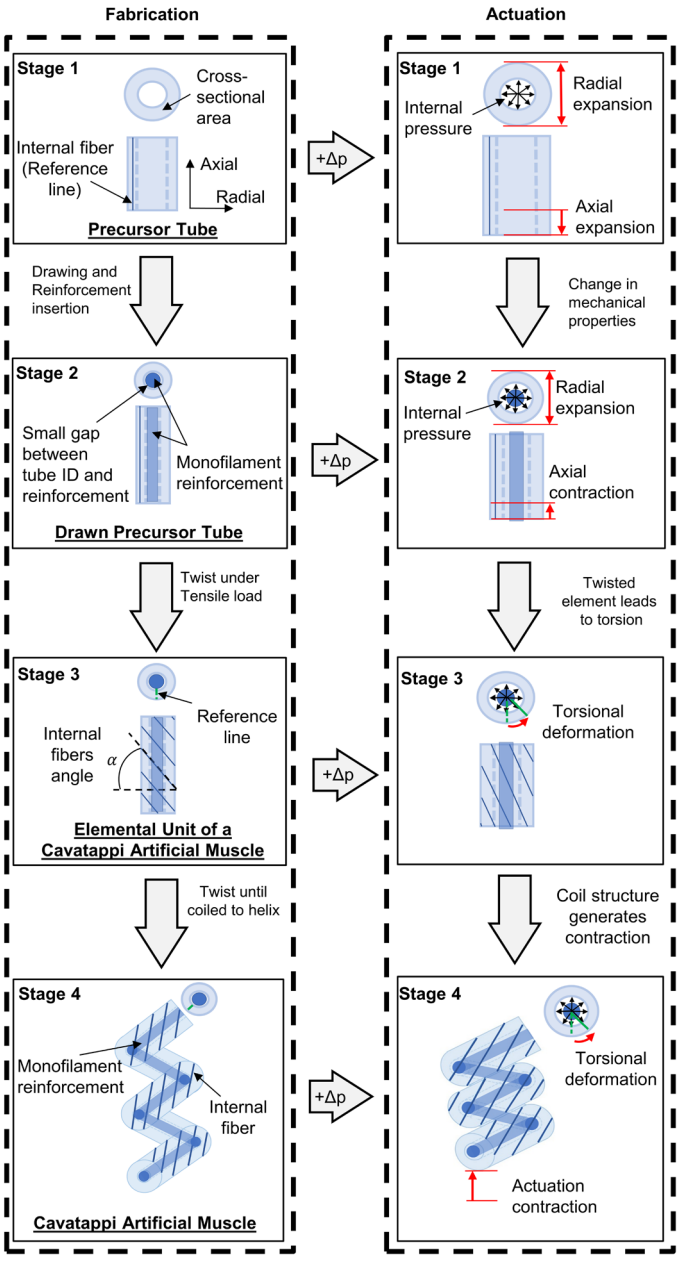

Fig. 3. Stages of fabrication of a cavatappi artificial muscle along with their actuation response at each stage. A blue reference line on the tube wall is used to track the actuation.

which is the time delay between input pressure and output actuation. This time lag of about 80 ms may be a result of viscoelasticity of the material or restriction to the fluid's flow through the small diameter tubes due to viscous shear, although further testing would be needed to verify this. This viscoelasticity is apparent in the actuation data of Fig. 4B between 0.25 and 1.6 s, where there is a steady increase in actuation, superimposed on the aforementioned ringing, under constant internal pressure. We hypothesize that during this time, the actuator diameter is steadily growing, causing not only (i) an increase in untwist of the tube but also (ii) an increase in effective spring stiffness due to changes in the polar moment of inertia of the tube cross section.

In addition, Fig. 4A does not show the maximum actuation strain generated during the conducted pressure ramp (Fig. 4B) because the actuation strain used to plot Fig. 4A is the data collected during the first ~0.25 s, measured after the 20 ms it takes for the material to respond; however, the muscle keeps contracting after this time. By comparing Fig. 4A with Fig. 4B, we see that the total actuation strain under a load of 0.4 kg is 16% after an actuation cycle of 1.5 s. This extra actuation strain seen in Fig. 4B compared with Fig. 4A is a result of various factors, such as the time lag and viscoelastic effects already mentioned and the inertial masses during actuation testing. Movie S2 shows the actuation responses under a load of 0.2 and 0.4 kg, respectively, where the dynamic actuation strain can be observed. Maintaining a steady high pressure on the cavatappi would produce actuation strains exceeding the results presented in either Fig. 4A or Fig. 4B as the tubes expand further.

Longer period actuation

With the knowledge of the PVC viscoelastic material response, a load of 0.4 kg was attached to a cavatappi after which a 240-psi pressure step was maintained for 5 min to observe longer-term actuation capacity. Here, the actuation response during the first 0.25 s is ~11%, which aligns with the actuation response in Fig. 4B. However, as time passes, the actuation strain increases substantially, but the rate of change tends toward zero. This is further evidence of the viscoelastic behavior of the material, which appears to be a first-order dynamic response to the step input. Figure 4C shows that after 5 min, the muscle develops 46% contraction, more than three times that after 0.25 s. This represents an increase in the work done by the actuator, which may have important applications where high strain is required, although the increased time reduces the actuator power.

Specific work and power

The time domain results of Fig, 4 (B and C) were used to calculate the specific work for these short- and long-term actuation modes to develop metrics to compare with other soft robotic actuator technologies (Table 1). The calculations are detailed in the Supplementary Materials but involve finding power and then integrating to get work. The short-term actuation response (0.25 s) developed a specific work of about 0.105 kJ/kg, whereas that of the long actuation response (5 min) was 0.38 kJ/kg.

Following the same methodology as the strain-time, another test was performed wherein velocity rather than position was measured to characterize the actuator's power. Figure 4D shows the peak and average velocities measured in these tests, as well as the calculated specific power results for various loads applied to the cavatappi. The applied internal pressure for these tests was 300 psi. The test with a 0.2-kg weight provided the highest peak and average power results of 1.42 kW/kg and 0.8 kW/kg, respectively, and therefore likely represents the mechanical matched-impedance at this input frequency. We should note that the pressure step occurred more than about 70 ms due to limitations in the regulator. The results in Fig. 4B show that about an 80-ms delay is expected between pressure application and actuation response. Hence, we believe that the specific power of cavatappi may be closer to two times the values presented above (2.84 and 1.6 kW/kg, respectively) but improved experimental setups would be required to validate the exact increase in the power. More details on the power calculation methods can be found in the Supplementary Materials.

Actuator lifetime

To assess actuator longevity, we conducted a 10,000 actuation cycle life test (500 of which are shown in Fig. 4E) of the cavatappi using a

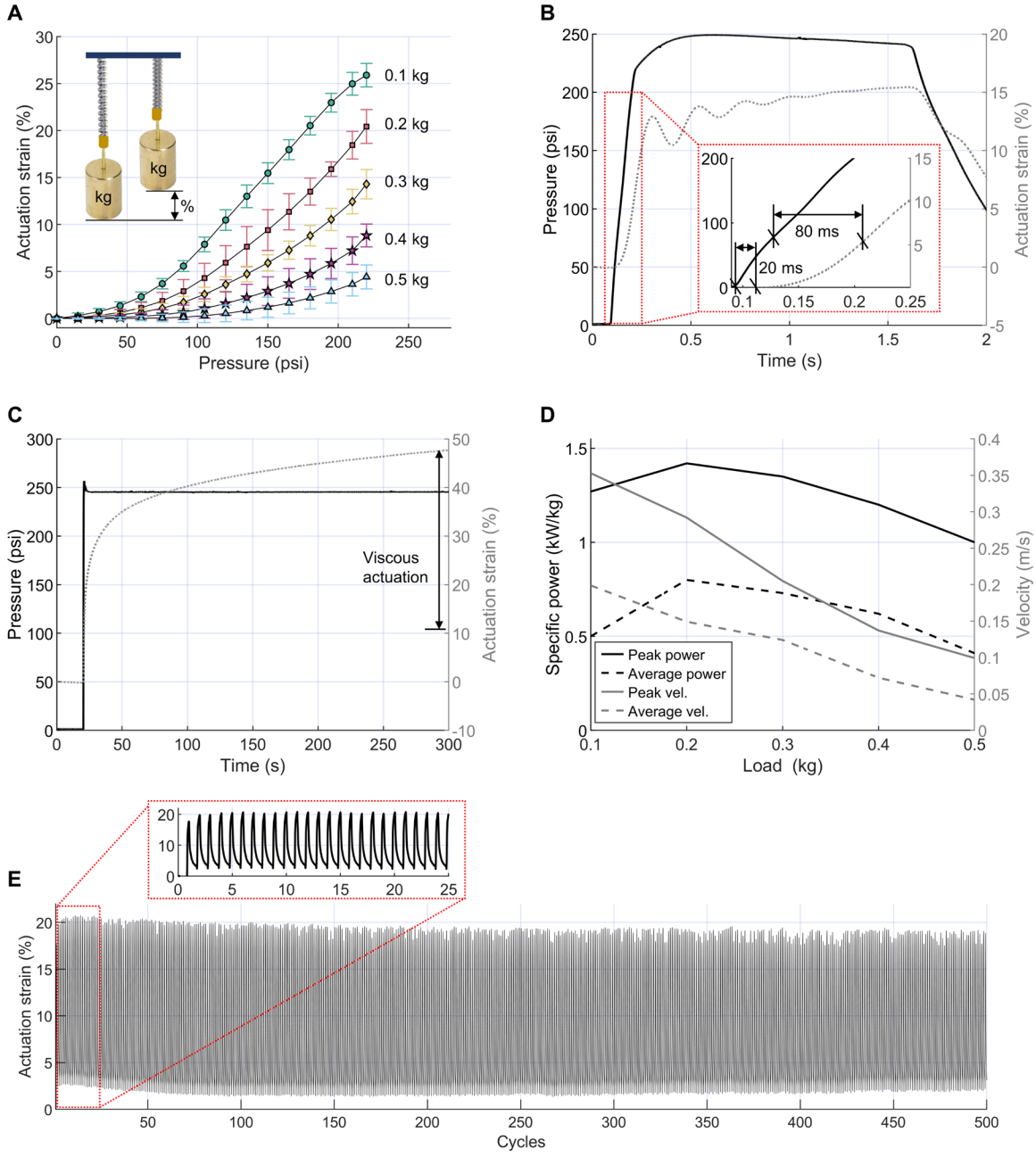

Fig. 4. Cavatappi artificial muscle actuation results. (**A**) Actuation strain as a function of pressure for 0.1-, 0.2-, 0.3-, 0.4-, and 0.5-kg applied tensile loads using a ramped pressure along with the 95% confidence intervals from data taken from trials on three different samples. (**B**) Pressure and actuation strain as a function of time under 0.4-kg tensile load. Inset is a zoomed image region of the first 0.25 s highlighting the response time and time lag. (**C**) Pressure and actuation strain as a function of time under 0.4-kg tensile load for a long period actuation cycle used to show actuation viscoelastic effects. (**D**) Peak and average specific power and velocity for 0.1-, 0.2-, 0.3-, 0.4-, and 0.5-kg tensile loads. (**E**) First 500 and 25 cycles of a 10,000-cycle lifetime test used to show first cycle effects and actuation creep. A cycle frequency of 1 Hz was limited by the regulator used for testing, not the bandwidth of the actuator itself.

0.2-kg load. The test concluded without failure or any sign of degradation, and the duration of the test was only limited by the size of the pressurized gas bottle used to actuate the cavatappi. Details related to this lifetime test can be found in the Supplementary Materials. Notice that the first 25 cycles in Fig. 4E also provide information on the viscous effects during the actuation recovery process of an actuation cycle. The recovery time seems to be about 2.5× the time it takes the actuator to contract. Such time recovery may be improved by using the prestretched configuration of cavatappi because this configuration does not depend on a bias load for recovery.

Application demonstrations

To illustrate the operability, applicability, fast actuation, energy storage, and precision control of cavatappi artificial muscles, we developed a number of demonstrations (see Figs. 5 and 6). In Fig. 5A, a single cavatappi artificial muscle is used to lift a 0.2-kg mass, and

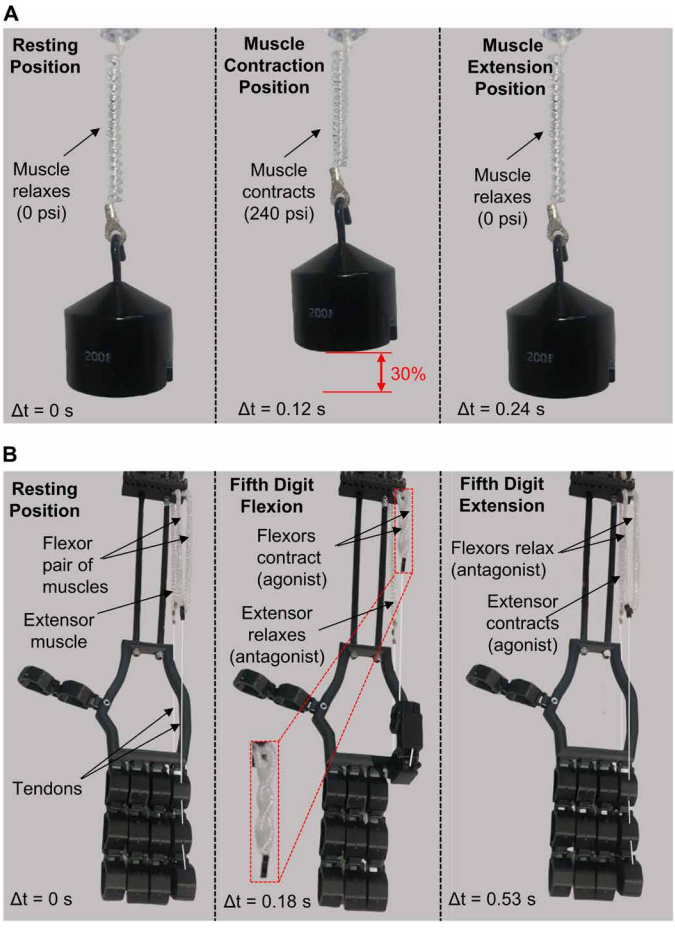

Fig. 5. Demonstration of the contraction response and biomimetic application of cavatappi artificial muscles. (**A**) Actuation strain cycle response for a 0.2-kg tensile load with a maximum internal pressure input of 240 psi. (**B**) Fifth digit actuation of a robotic hand using two cavatappi artificial muscles as the flexor muscles and one as the extensor muscle.

in Fig. 5B, cavatappi flexor and extensor muscles are used to actuate a robotic digit. Both Figs. 5A and 5B are time frames that have been extracted from movies S2 and S5, respectively, which highlight the speed of actuation. The basic actuation demonstration in Fig. 5A used a single cavatappi artificial muscle that was cyclically actuated with 240-psi air under a tensile load of 0.2 kg. A fast-opening valve was manually triggered such that an entire contraction and expansion cycle required only 0.24 s (~4 Hz). Under these actuation conditions, the muscle generated an axial contraction of ~30%. Figure 5A also shows that at a pressure of 240 psi, the maximum actuation response was limited by the saturation of the cavatappi coils, and thus, higher pressures would do little to change the performance.

Whereas the muscle shown in Fig. 5A was fabricated without an initial prestretch, movie S2 also shows a second similar muscle fabricated with prestretched and actuated under the same axial load of 0.2 kg. During fabrication, this muscle was stretched by 130% and thermally annealed at 190°F for 30 min, before cooling under room temperature conditions to maintain the stretched configuration after removal of the mechanical restraints. That cavatappi contracted 40% during actuation, an increase of 10% more than the unstretched muscle. The extra 10% actuation response shown in movie S2 is attributed to the prestretched configuration, which delays muscle saturation. Movie S2 also shows the same prestretched cavatappi artificial muscle but under an axial load of 0.4 kg. Under this condition, the sample contracts 16% with a pressure of 240 psi; a similar result was found using unstretched muscle because under this higher applied load, neither muscle contracts enough to saturate.

Following others (*17*, *34*), we three-dimensionally printed a robotic hand with dimensions similar to those of an adult human to show the biomimetic potential of cavatappi (Fig. 5B). The cavatappi were placed on this model to allow for flexion and extension of only the fifth digit. Cavatappi could have also been placed on the other digits to develop a fully functional robotic hand, but they were excluded in this work for image clarity. Like human hands, each finger was composed of three segments. The pinky (or fifth digit) shown in Fig. 5B was actuated by the contraction of two parallel cavatappi artificial muscles placed in the interior forearm, mimicking those muscles in a human arm, with restorative forces induced by a single antagonistic cavatappi on the posterior of the arm. Both flexors and extensor muscles were prestretched cavatappi. The linear actuation was transmitted to the tip of the finger by a 0.2-mm-diameter monofilament nylon tendon.

In the resting position, the flexor and extensor muscles were set into an extended position of the fifth digit (Fig. 5B, Resting Position), and all had an internal pressure of 0 psi. To actuate, pressure was cycled between 0 and 240 psi by opening and closing a pneumatic valve. During the finger flexion, the flexors rapidly contracted in 0.18 s. This contraction also led to an extension in the extensor muscle (Fig. 5B, Flexion). As shown in the inset of Fig. 5B, during flexion, the flexors not only contract but also helically wrap around each other as a result of the untwist that occurs on the sample, leading to an increase in the finger flexion. The secondary helical twisting of the actuator around each other provided additional path length and contraction as a result, beyond what would be expected from a single cavatappi. After the flexion, the flexors were depressurized, and the extensor was pressurized. This induced extension of the finger (Fig. 5B, Extension), at which point, both muscles were depressurized. Figure 5B also shows the actuation time for a cycle (finger flexion and extension) to be about half of a second (~2 Hz).

To emphasize high precision actuation and potential elastic energy storage capacity (strain energy), Fig. 6 (A and B) shows actuation of a mechanical arm via a linear-parallel configuration of nine cavatappi (the same cavatappi shown in Fig. 1C with the configuration shown in Fig. 1H). In Fig. 6A (movie S7), a laser pointer is attached to the end of the arm. The laser pointer illuminates a red dot on the black background in Fig. 6A, where three different targets were set (bottom, middle, and top targets as shown in Fig. 6A). As previously mentioned, the mechanical arm was actuated using a linear-parallel configuration of nine cavatappi; to generate initial stretching of the muscle, a bias mass of 0.2 kg was hung from the platform where the laser was sitting, although prestretched muscles could have been used. At the initial position, the muscles were slightly pressurized (50 psi) to aim the laser at the bottom target. After ~3 s, the internal pressure was increased to 200 psi, moving the arm to illuminate the top target (position 1 in Fig. 6A), after which the arm was controlled to illuminate the middle target.

The strain energy stored in an ideal helical spring is $\frac{1}{2}kx^2$, where k is the spring constant and x is the deflation of the spring from its equilibrium position. The helical shape of cavatappi invites the application of this standard model, albeit with variable stiffness and

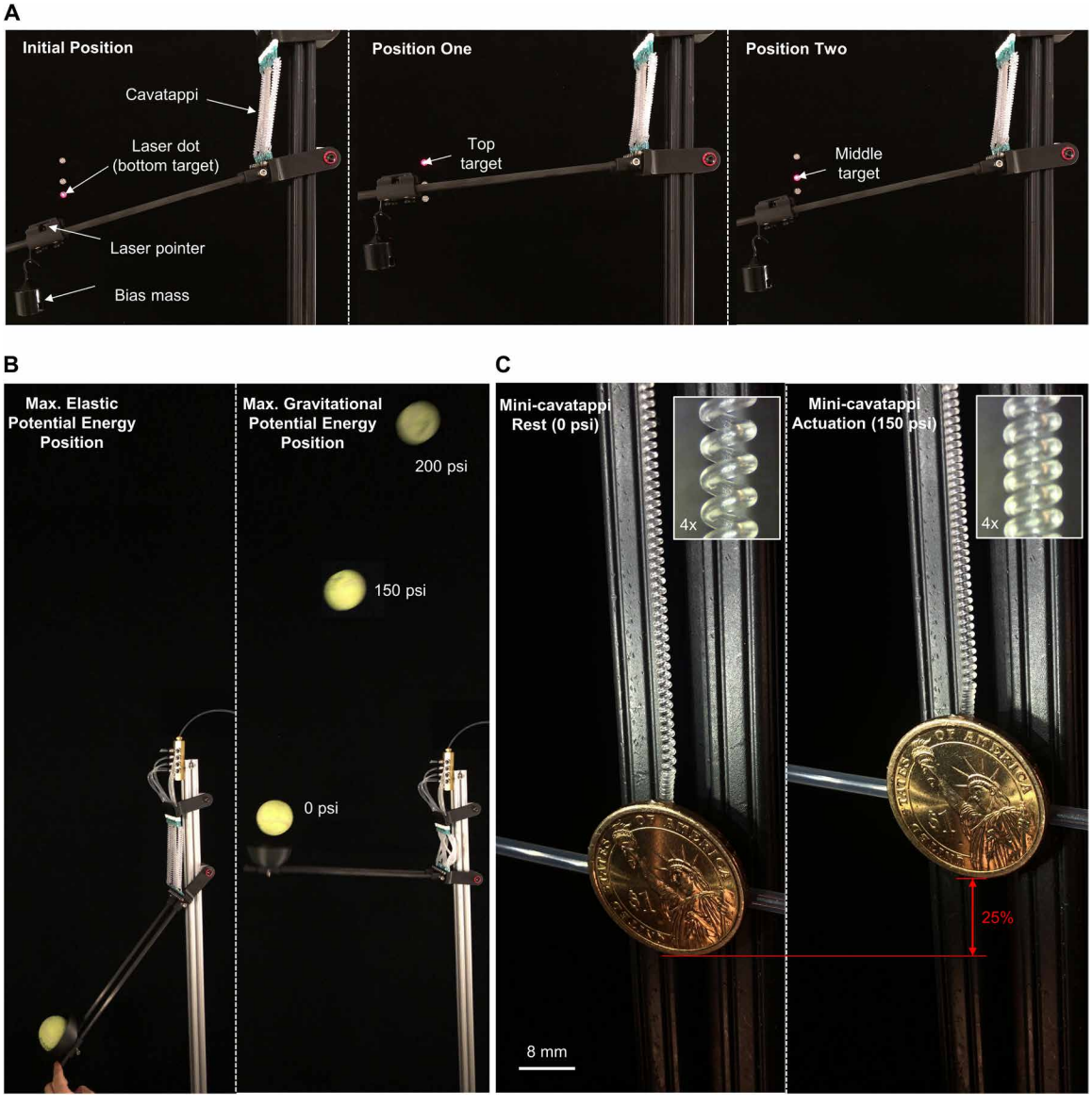

Fig. 6. Applications of cavatappi artificial muscles to show the precise actuation, elastic energy storage, and scalability properties. (**A**) High precision actuation strain for a linear-parallel configuration of nine cavatappi used to aim at three different targets with a laser pointer attached to the actuated arm. (**B**) Same application shown in (A) used to highlight the potential elastic energy storage capacity of cavatappi. (**C**) Actuation response developed by the mini-cavatappi shown in Fig. 1F under a load of 8.1 g (dollar coin).

equilibrium positions in response to pressure. Hence, it is clear that cavatappi have an inherent energy storage capacity that, like human muscle, can be used to increase the actuation cycle efficiency in applications such as robotic running (*35*). This effect is highlighted in Fig. 6B (movie S6), wherein the arm of Fig. 6A is adapted to hold a standard tennis ball. In this test, the linear-parallel cavatappi configuration was initially stretched to store strain energy and subsequently released to launch a tennis ball. This experiment was repeated at pressures of 0, 150, and 200 psi to vary both the actuator stiffness and equilibrium position and thus store varying energy for a given arm angle. The maximum gravitational potential energy position illustrates the maximum height that the tennis ball reached under the above specified pressures. Here, it observed an increase in gravitational potential energy as the pressure increases; at a pressure of 200 psi, the tennis ball exited the frame of the recorded video; thus, it is shown before departure in Fig. 6B.

One more interesting feature of cavatappi artificial muscles are the potential to be scaled down. The limits on miniaturization of these devices are primarily related to the manufacturing limits of the precursor tube. One might initially think that miniaturization of the tube would decrease the flow, which is needed to inflate the actuators because of viscous losses, but the required inflation flow rate in these actuators scales by the square of the internal diameter. The average velocity in a laminar flow scales in the same way for a given applied pressure gradient. We therefore do not expect substantial bandwidth limits associated with viscous losses when miniaturized. To highlight the capacity for miniaturization, we reduced the size of the principal cavatappi studied in this work (Fig. 1C) by 2.5× through

the use of a tube with 250 μm *ID* and 700 μm *OD* (Fig. 1F). Figure 6C and movie S4 show the actuation response of this mini-cavatappi under the tensile load generated by a coin that was glued to the end of the muscle. Under this load, the mini-cavatappi contracted 25% when a pressure of 150 psi was internally applied. Figure 6C also shows a 4× zoomed image of the coiled section, which highlights the change in pitch of the helical structure during actuation.

Preliminary modeling of cavatappi artificial muscles

Our initial modeling efforts focus on the variation in the cavatappi stiffness and free length in response to internal pressure changes. We know from classical mechanics theory that the torsional stiffness of a hollow tube can be related to the internal and external diameters via

$$k_t = \frac{\pi G}{32l}(OD^4 - ID^4) \quad (1)$$

Here, G is the material's shear modulus, l is the length of the tube, and OD and ID are the outer and inner diameters of the tube, respectively. Note that Eq. (1) neglects viscous effects. Although we have shown viscoelastic effects to be present in cavatappi, for high bandwidth actuation, these effects would be relatively small. In addition, the internal material damping, apparent in the exponential decay of the ringing response in Fig. 4B, is relatively small.

If we assume that the wall thickness does not change substantially during internal pressurization (only because of Poisson's effect) and add a change in diameter, Δd, to both the OD and ID terms, then we get a fourth-order polynomial for stiffness k as a function of Δd. Under certain conditions, e.g., when $0 < \Delta d/OD < 1$ and $ID \sim OD/2$, which reasonably approximates the conditions for the experiments in this work, the fourth-order polynomial for k can be approximated as linear. Given this result, we can see that the torsional stiffness of an inflating tube like a cavatappi scales approximately with the relationship $k_t = k_{t0} + c_t \Delta d$, where k_{t0} is the original torsional stiffness and c_t is a constant of proportionality. Figure 2A shows a relatively linear relationship between pressure and diameter, and therefore, the stiffness can also be considered linear in pressure. The torsional stiffness of such a straight tube is directly related to the linear stiffness of a coiled helical spring, and hence, the cavatappi spring stiffness could be modeled as two springs in parallel, one with some initial stiffness (k_0) and one with a stiffness linearly dependent on pressure (k_p).

In addition to stiffness changes, the free length of the cavatappi changes during pressurization. A prestretched cavatappi with no hanging weight contracts to a new free position when pressurized. This change in length is a result of the local untwisting of the elemental sections. We have shown in our work on TPAs that for a given radial layer, the amount of untwist, and therefore free contraction, is linearly related to the radial strain (*21*). To first order, this radial strain is related linearly to internal pressure. It is therefore reasonable to assume that the free retraction length (δx_f) of these actuators is linearly related to internal pressure, a fact verified for pressures above ~60 psi in Fig. 4A for the lightest load applied (0.1 kg). However, this figure also shows that more advanced nonlinear modeling would be needed for less pressure or higher loads.

If we include a deviation from this initial position x, we can develop an actuator force model for a cavatappi, that is

$$F_c = (k_0 + k_p)(x + \delta x_f) \quad (2)$$

Here, k_0 is the initial cavatappi spring stiffness, k_p is the stiffness changes due to pressurization, δx_f is the free retraction length for the applied pressure, and x is the displacement of the end of the actuator from its initial position. As previously mentioned, it is likely that both k_p and δx_f are linearly related to pressure and could therefore be easily modeled for a given actuator. Even if nonlinearities are present, they could also be modeled or empirically derived to apply the actuator model in Eq. (2). Future work will be needed to include viscoelastic effects on stiffness and free retraction lengths, as well as a modeling effort to understand how internal damping is affected by internal pressure and the resulting tube diametral changes. We saw in Fig. 4 (B and C) that the work and power capacities of these devices are input frequency–dependent, so we expect that damping terms may be needed in Eq. (2) to accurately predict this time dependence. In addition, the internal material damping apparent in the exponential decay of the ringing response in Fig. 4B shows that advanced modeling will need to include damping.

DISCUSSION

Here, we have introduced a low-cost, lightweight, fluidic artificial muscle whose actuation relies upon (i) the anisotropic physical properties introduced into the virgin material through extrusion and enhanced by a cold drawing process, (ii) the reorientation of those properties through a twisting or twisting and coiling process, and (iii) the deformation of the reconfigured material through the application of an internal pressure. The flexibility of cavatappi will allow them to be used on applications over corners/joints such as a knee, elbow, or ankle, because they can be placed under a curved deformation and still actuate. Their simplicity also presents an advantage in applications. Because cavatappi are fabricated from soft PVC tubing, the same tube length could consist of sections where the drawn precursor tube is coiled-twisted, straight-twisted, or simply kept as the original straight drawn configuration. Hence, a single tube length with a coiled section in the middle could serve as (i) the plumbing from the pressure source, (ii) the actuator, and (iii) the tendon running to the point of force application. Such an implementation would decrease the overhead mass and complexity from fittings, increase reliability by eliminating leaks, and decrease maintenance.

The data collected and testing presented herein for cavatappi can be used to develop performance metrics that can be compared with similar actuator technologies. The data in Table 1 compare cavatappi with other soft robotic technologies. In addition to Table 1, Fig. 7 also provides quick comparisons between cavatappi artificial muscles and PPAMs, TPAs, and human skeletal muscles for a variety of performance metrics often reported for artificial muscles: average specific power and specific work, response time, maximum stress and strain, and total contractile efficiency. Once again, we consider cavatappi to be, to an extent, a hybrid configuration between TPAs and PPAMs; thus, Fig. 7 compares these and human skeletal muscles. We should note that the response times presented in the spider graph are somewhat subjective estimates of the authors based on the actuation driver. The exact response time depends on the details of the driver (for example, a much faster actuation response can be obtained in thermally activated TPAs when is applied via conduction, as compared with convection), so only categories of response times are presented.

Both Fig. 7 and Table 1 show that TPAs present high specific work and power as well as high maximum stress and strain, which

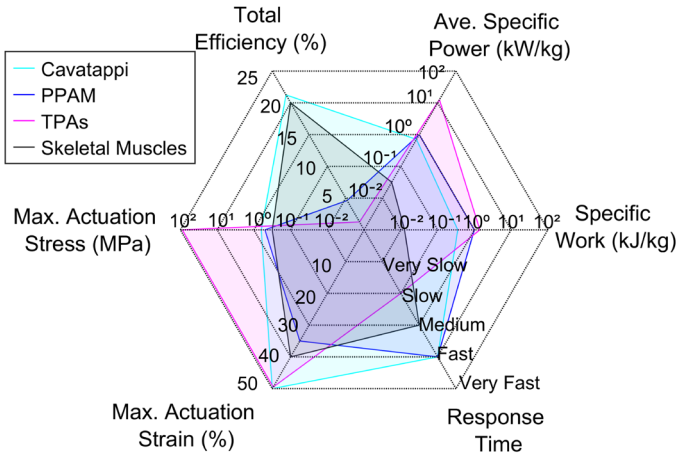

Fig. 7. Artificial muscles performance comparison along with those of skeletal muscles (*1*, *2*–*6*, *16*, *20*–*22*).

has led to notable research interest, yet their thermal activation limits their total efficiency and response time. PPAMs show similar maximum actuation stress and strain properties as human muscles but outperform human muscles in specific power, work, and response time. Because they are also pressure driven, similar actuation properties are found for cavatappi artificial muscles as those for PPAMs; however, cavatappi artificial muscles are shown to exceed PPAMs maximum actuation strain and the total system efficiency. Furthermore, when compared with PPAMs, cavatappi artificial muscles are inexpensive ($0.9/m of cavatappi muscle), and because cavatappi fabrication processing embeds similar microstructural anisotropy developed through macroscale features in PPAMs, they are far simpler to fabricate yet develop similar specific power and work metrics. Moreover, PPAMs expand drastically in the radial direction during actuation. Cavatappi bypass this pitfall, relying upon an internal microstructure for anisotropy and developing relatively little helix diametral deformation during actuation (see Fig. 5, A and C).

As we see in Fig. 7, cavatappi artificial muscles are capable of mimicking some human muscle properties and outperforming others, such as fast contraction activation, specific power and work, and maximum force and contraction. Furthermore, like human skeletal muscles, cavatappi artificial muscles have the potential for stacking in parallel to increase force generation (see movies to S7). We have demonstrated parallel operation here: Nine cavatappi artificial muscles of the same length were connected in parallel to increase the generated torque by nine times on the arm in Fig. 6B. Extending this concept, cavatappi could be bundled similarly to that of biological muscle bundles, as shown in Fig. 1G.

The maximum actuation strain of cavatappi is somewhat limited by the bursting pressure, which we think is related to the ultimate strength of the drawn PVC material in the direction perpendicular (transverse) to the tie-chain molecules running in the helical direction around our actuators. The observed failure mode is one in which bursting occurs in tiers parallel to the draw direction. Increasing wall thickness increase would increase burst pressure but at the expense of diametral expansion and proportionally higher pressure for a given amount of actuation. Similarly, increasing the amorphous region tensile limit would likely lead to increased burst pressure, but work in this area would need to ensure that the modulus in the hoop direction was not also increased, as doing so would adversely affect actuation.

We have used soft PVC to fabricate these actuators, but there may be polymers with the right combination of anisotropy and radial compliance after cold drawing needed for cavatappi-type actuation, and there may be polymers that allow for a larger maximum pressure or actuate more efficiently. We tested some nylon and polyurethane tubes, but we found that nylon had a hoop stiffness too high to actuate at the pressures that we were able to apply and that polyurethane was so weak radially that it failed at relatively low internal pressures. Although this limited material study used PVC, we have no reason to believe that this is the only material that can serve as cavatappi. On the contrary, we believe that cavatappi can be optimized by designing and/or selecting precursor materials that maximize anisotropic properties and allow those properties to reorient with twisting/coiling.

Reducing pressure required for a given amount of actuator strain should be a primary future goal of this technology, but it is fundamentally a question of actuator efficiency. To reduce the amount of required pressure for a given actuation strain, the actuator efficiency would need to be increased because pressure is directly related to the input work. We have demonstrated an actuator contractile efficiency of about 45%, which is similar to related technologies. If a material could be found that has a lower transverse modulus, then high pressure could be traded for larger requirements on pumped internal volume while maintaining this high actuator efficiency. Doing so though would necessarily increase the rate of tube expansion and therefore more quickly saturate the muscle, thus potentially reducing the actuator stroke and specific work capacity. The wall thickness to inner diameter ratio could potentially be reduced to increase the diametral deformation in response to internal pressure and thereby increase efficiency, but it is critical that the ratio is not reduced so far that the tubes can kink during twisting, which would, in turn, prevent the actuator fluid flow through the entire actuator length. This "kink" stability is a critical design objective of future optimization, although the reinforcing monofilaments would help to prevent this failure mode. The tubes used in this work have used a predrawn *OD*/*ID* ratio of 2.1/2.8, which has resulted in tubes that have yet to fail to actuate due to kinking.

More extensive material modeling of cavatappi would highlight some of these trade-offs and how material properties directly affect actuation performance. Expanding and validating the model of cavatappi artificial muscle presented in this work will be the subject of future work; however, compared with TPAs, it will be substantially simpler because only the mechanical properties of the precursor tube are needed, and there is a reduced need to collect mechanical properties as a function of temperature. Furthermore, the soft PVC used for our cavatappi presents small moisture absorption (*36*); thus, moisture dependencies would not need to be included in actuation models, unlike nylon TPAs, which require material models that include thermal and hydroscopic effects (*27*). The modeling of PVC cavatappi artificial muscles will need to follow a linear viscoelastic characterization due to the viscoelastic effects that are reported in this work. Last, we expect that future work will include the use of cavatappi artificial muscles in many applications due to their simplicity, low-cost, lightweight, flexibility, efficiency, and strain energy recovery properties, among other benefits.

MATERIALS AND METHODS

The material used throughout this work is Soft ND-100-65 Tygon PVC tubing. As described in section S1, cold drawing, twisting, and

coiling of this PVC tubing make the cavatappi artificial muscle. The results presented in this work use the cavatappi in Fig. 1C with linear density of 0.014 g/mm and dimensions in fig. S2 (except the mini-cavatappi was used in Fig. 6C and movie S4). This cavatappi was reinforced with an internal nylon monofilament inserted into the hollowed tube during fabrication (see section S1). The reinforcement was found to reduce a pinching-type failure mode observed in life-cycle testing. In addition, it was found that over thousands of cycles, actuation creep was observed for cavatappi without a reinforcement. The reinforcing monofilament provided a restoring force after pressure was removed, which helped to reduce actuation creep.

For all actuation tests and metrics calculations performed in this work, we used a Polytec OFV-5000 Vibrometer controller with the OFV-534 optics head. To apply and measure pressure in these tests, we used a RG1262-1500 pressure regulator along with QB1T closed-loop servo system and a DS-series pressure transducer from Proportion-Air. The voltage outputs of these systems are linearly related to a change of position of the object on which it focuses (vibrometer) and change in pressure (pressure transducer) (fig. S3). This voltage was recorded by a National Instruments PXIe-6361 multifunction data acquisition card and subsequently analyzed to develop the data presented in this work. More details on testing methods and calculations of metrics in Table 1 and Fig. 7 are found in the Supplementary Materials.

SUPPLEMENTARY MATERIALS

robotics.sciencemag.org/cgi/content/full/6/53/eabd5383/DC1
Materials and Methods
Fig. S1. Fabrication and processing of a cavatappi artificial muscle and its elemental unit.
Fig. S2. Side, cross-sectional, and top views of a cavatappi along with its dimensions.
Fig. S3. Experimental setups used to measure axial strain of the precursor tube, radial strain for the precursor tube, the torsional actuation of an elemental unit of a cavatappi, and the axial actuation of a cavatappi artificial muscle.
Fig. S4. Pressure-volume curve used to calculate the energy in during an actuation contraction and force-displacement used to calculate the work generated during an actuation contraction.
Fig. S5. Actuation under a load of 1.1 kg to show the maximum stress and under a load of 0.1 kg to show maximum strain.
Fig. S6. The torsional actuation of a cavatappi artificial muscle elemental unit.
Table S1. Values obtained from fig. S4.
Movie S1. Mechanism of cavatappi actuation.
Movie S2. Cavatappi actuation.
Movie S3. Prestretched cavatappi actuation under no load.
Movie S4. Mini-cavatappi actuation.
Movie S5. Fifth digit flexion and extension of a robotic hand.
Movie S6. Strain potential energy storage.
Movie S7. High controllability.

REFERENCES AND NOTES

1. C. S. Haines, M. D. Lima, N. Li, G. M. Spinks, J. Foroughi, J. D. Madden, S. H. Kim, S. Fang, M. J. de Andrade, F. Goktepe, S. M. Mirvakili, S. Naficy, X. Lepro, J. Oh, M. E. Kozlov, S. J. Kim, X. Xu, B. J. Swedlove, G. G. Wallace, R. H. Baughman, Artificial muscles from fishing line and sewing thread. *Science* **343**, 868–872 (2014).
2. B. Tondu, P. Lopez, The McKibben muscle and its use in actuating robot-arms showing similarities with human arm behavior. *Industrial Robot. Int. J.* **24**, 432–439 (1997).
3. P. Ohta, L. Valle, J. King, K. Low, J. Yi, C. G. Atkeson, Y.-L. Park, Design of a lightweight soft robotic arm using pneumatic artificial muscles and inflatable sleeves. *Soft Robot.* **5**, 204–215 (2017).
4. C. Ching-Ping, B. Hannaford, Measurement and modeling of McKibben pneumatic artificial muscles. *IEEE Trans. Robot. Autom.* **12**, 90–102 (1996).
5. F. Daerden, D. Lefeber, B. Verrelst, and R. Van Ham, Pleated pneumatic artificial muscles: compliant robotic actuators, in *Proceedings 2001 IEEE/RSJ International Conference on Intelligent Robots and Systems* (2001), vol. 4.
6. D. Villegas, M. Van Damme, B. Vanderborght, P. Beyl, D. Lefeber, Third–generation pleated pneumatic artificial muscles for robotic applications: Development and comparison with McKibben muscle. *Adv. Robot.* **26**, 1205–1227 (2012).
7. S. Kurumaya, K. Suzumori, H. Nabae, S. Wakimoto, Musculoskeletal lower-limb robot driven by multifilament muscles. *Robomechanical* **3**, 18 (2016).
8. R. V. Ham, T. G. Sugar, B. Vanderborght, K. W. Hollander, D. Lefeber, Compliant actuator designs. *IEEE Robot. Autom. Mag.* **16**, 81–94 (2009).
9. R. Niiyama, X. Sun, C. Sung, D. Rus, S. Kim, Pouch motors: Printable soft actuators integrated with computational design. *Soft Robot.* **2**, 59–70 (2015).
10. N. Oh, Y. J. Park, S. Lee, H. Lee, H. Rodrigue, Design of paired pouch motors for robotic applications. *Adv. Mater. Technol.* **4**, 1800414 (2019).
11. S. Li, D. M. Vogt, D. Rus, R. J. Wood, Fluid-driven origami-inspired artificial muscles. *Proc. Natl. Acad. Sci.* **114**, 13132, 13137 (2017).
12. J.-G. Lee, H. Rodrigue, Origami-based vacuum pneumatic artificial muscles with large contraction ratios. *Soft Robot.* **6**, 109–117 (2019).
13. J. G. Lee, H. Rodrigue, Efficiency of origami-based vacuum pneumatic artificial muscle for off-grid operation. *Int. J. Precis. Eng. Manuf. Green Technol.* **6**, 789–797 (2019).
14. E. Acome, S. K. Mitchell, T. G. Morrissey, M. B. Emmett, C. Benjamin, M. King, M. Radakovitz, C. Keplinger, Hydraulically amplified self-healing electrostatic actuators with muscle-like performance. *Science* **359**, 61–65 (2018).
15. N. Kellaris, V. Gopaluni Venkata, G. M. Smith, S. K. Mitchell, C. Keplinger, Peano-HASEL actuators: Muscle-mimetic, electrohydraulic transducers that linearly contract on activation. *Sci. Robot.* **3**, eaar3276 (2018).
16. L. Wu, Y. Tadesse, Musculoskeletal System for Bio-Inspired Robotic Systems Based on Ball and Socket Joints, in *ASME International Mechanical Engineering Congress and Exposition* (2016), vol. **4A**.
17. M. Yip, G. Niemeyer, High-Performance Robotic Muscles from Conductive Nylon Sewing Thread, in *Proceedings - IEEE International Conference on Robotics and Automation* (2015), pp. 2313–2318.
18. J. Sun, B. Tighe, Y. Liu, J. Zhao, Twisted-and-coiled actuators with free strokes enable soft robots with programmable motions. *Soft Robot.* **0**, (2020).
19. J. D. W. Madden, S. Kianzad, Twisted Lines: Artificial muscle and advanced instruments can be formed from nylon threads and fabric. *IEEE Pulse* **6**, 32–35 (2015).
20. M. Hiraoka, K. Nakamura, H. Arase, K. Asai, Y. Kaneko, S. W. John, K. Tagashira, A. Omote, Power-efficient low-temperature woven coiled fibre actuator for wearable applications. *Sci. Rep.* **6**, 36358 (2016).
21. A. M. Swartz, D. R. H. Ruiz, M. Shafer, H. Feigenbaum, C. C. Browder, Experimental characterization and model predictions for twisted polymer actuators in free torsion. *Smart Mater. Struct.* **27**, 114002 (2018).
22. M. W. Shafer, H. P. Feigenbaum, D. Pugh, M. Fisher, First steps in modeling thermal actuation of twisted polymer actuators using virgin material properties, in *ASME 2016 Conference on Smart Materials, Adaptive Structures and Intelligent Systems, American Society of Mechanical Engineers* (2016), vol. 2.
23. D. R. Higueras-Ruiz, C. J. Center, H. P. Feigenbaum, A. M. Swartz, M. W. Shafer, Finite element analysis of straight twisted polymer actuators using precursor properties. *Smart Mater. Struct.* **30**, 025005 (2020).
24. M. Shafer, H. Feigenbaum, D. Higueras Ruiz, A novel biomimetic torsional actuator design using twisted polymer actuators. *Smart Mater.* **1**, 7 (2017).
25. D. R. Higueras Ruiz, "Characterizing material properties of drawn monofilament for twisted polymer actuation," thesis, ProQuest. Northern Arizona University (2018).
26. A. M. Swartz, "Characterization and modeling of drawn polymers and twisted polymer actuators," thesis, ProQuest. Northern Arizona University (2019).
27. D. Higueras Ruiz, H. Feigenbaum, M. Shafer, Moisture's significant impact on twisted polymer actuation. *Smart Mater. Struct.* **29**, 125009 (2020).
28. S. Aziz, S. Naficy, J. Foroughi, H. R. Brown, G. M. Spinks, Controlled and scalable torsional actuation of twisted nylon 6 fiber. *J. Polym. Sci. B Polym. Phys.* **54**, 1278–1286 (2016).
29. S. Sharafi, G. Li, A mutliscale approach for modeling actuation response of polymeric artificial muscle. *Soft Matter* **11**, 3833–3843 (2015).
30. K. Farzad, T. Yonas, Modeling of twisted and coiled polymer (TCP) muscle based on phenomenological approach. *Smart Mater. Struct.* **26**, 125010 (2017).
31. R. G. C. Arridge, P. J. Barham, A theory for the drawing of oriented crystalline polymers. *J. Polym. Sci. Polym. Phys. Ed.* **16**, 1297–1319 (1978).
32. D. Prevorsek, P. Harget, R. Sharma, A. Reimschuessel, Nylon 6 fibers: changes in structure between moderate and high draw ratios. *J. Macromol. Sci. Part B Phys.* **8**, 127–156 (1973).
33. A. Peterlin, Plastic deformation and structure of extruded polymer solids. *Polym. Eng. Sci.* **14**, 627–632 (1974).
34. F. A. Mohd, J. Ooga, T. Goto, K. Takeichi, M. Suzumori, Index finger of a human-like robotic hand using thin soft muscles. *IEEE Robot. Autom. Lett.* **3**, 92–99 (2018).
35. S. Seok, A. Wang, Meng Yee Chuah, D. Otten, J. Lang and S. Kim, Design principles for highly efficient quadrupeds and implementation on the MIT Cheetah robot, in *2013 IEEE International Conference on Robotics and Automation* (2013), pp. 3307–3312.

36. TYGON ND 100–65 Medical Tubing, 2011. Saint-Gobain Performance Plastic; https://usplastic.com/catalog/files/specsheets/TYGON_ND_100-65.pdf (accessed April 04, 2020).
37. FLIGHT WORKS Inc. M-Series (Magnetic Drive Gear Pumps), MODELS 2232-M04C10/C12/C15 (Irvine, CA); http://products.flightworksinc.com/Asset/Product%20Data%20Sheet%20(2232-M04C10.C12.C15).pdf [accessed 7 February 2021].
38. Dr. Eric Besnard, President and CEO of FLIGHT WORKS, Inc. (09/29/2020). Quoting M-Series Brushless micro-pumps efficiency (On-line meeting).
39. MICROPUMP, Health & Science. Series GAF (External Gear Pumps) (Vancouver, WA); https://micropump.com/support_documents/gaf_tech_specs.pdf [accessed 7 February 2021].
40. TOPSFLO, MG200XK&DC24, (Magnetic Drive Gear Pumps) (Changsha City, Hunan); http://topsflo.com/micro-gear-pump/mg200xk-dc24.html [accessed 7 February 2021].
41. M. Meller, J. Chipka, A. Volkov, M. Bryant, E. Garcia, Improving actuation efficiency through variable recruitment hydraulic {McKibben} muscles: modeling, orderly recruitment control, and experiments. *Bioinspir. Biomim.* **11**, 065004 (2016).
42. D. Sutton, J. Kimm, Reaction time of motor units in biceps and triceps. *Exp. Neurol.* **23**, 503–515 (1969).
43. J. D. W. Madden, N. A. Vandesteeg, P. A. Anquetil, P. G. A. Madden, A. Takshi, R. Z. Pytel, S. R. Lafontaine, P. A. Wieringa, I. W. Hunter, Artificial muscle technology: Physical principles and naval prospects. *IEEE J. Ocean. Eng.* **29**, 706–728 (2004).

Funding: This work has been conducted at the Dynamic Active Systems Laboratory and supported by the Northern Arizona University's Research and Development Preliminary Studies grant. **Author contributions:** D.R.H.-R., H.P.F., and M.W.S. jointly conceived the presented actuator concept. D.R.H.-R. designed the experiments, manufactured the devices, collected the data, performed the analysis, wrote the manuscript, and created the movies. H.P.F and M.W.S. advised on all parts of the project and reviewed the manuscript. **Competing interests:** The authors declare that they have no competing interests. A provisional patent application has been filled relating to this work by the Northern Arizona University. U.S. Provisional Patent application no. 63036750, filed 9 June 2020. **Data and materials availability:** All data needed to support the conclusions of this manuscript are included in the main text or the Supplementary Materials. Other materials can be found at http://openknowledge.nau.edu/id/eprint/5533.

Submitted 30 June 2020
Accepted 26 March 2021
Published 21 April 2021
10.1126/scirobotics.abd5383

Citation: D. R. Higueras-Ruiz, M. W. Shafer, H. P. Feigenbaum, Cavatappi artificial muscles from drawing, twisting, and coiling polymer tubes. *Sci. Robot.* **6**, eabd5383 (2021).

Science Robotics

Cavatappi artificial muscles from drawing, twisting, and coiling polymer tubes

Diego R. Higueras-Ruiz, Michael W. Shafer, and Heidi P. Feigenbaum

Sci. Robot. **6** (53), eabd5383. DOI: 10.1126/scirobotics.abd5383

Science Robotics (ISSN 2470-9476) is published by the American Association for the Advancement of Science. 1200 New York Avenue NW, Washington, DC 20005. The title *Science Robotics* is a registered trademark of AAAS.